

## Multiplexing-oriented plasmon-MoS<sub>2</sub> hybrid metasurfaces driven by nonlinear quasi bound states in the continuum: supplement

QUN REN,<sup>1</sup>  FENG FENG,<sup>2,8</sup> XIANG YAO,<sup>3</sup> QUAN XU,<sup>2</sup>  MING XIN,<sup>1,9</sup> ZHIHAO LAN,<sup>4</sup> JIANWEI YOU,<sup>4,5</sup>  XIAOFEI XIAO,<sup>6</sup>  AND WEI E. I. SHA<sup>7,10</sup> 

<sup>1</sup>*School of Electrical and Information Engineering, Tianjin University, Tianjin, 300072, China*

<sup>2</sup>*School of Precision Instruments and Opto-Electronics Engineering, Tianjin University, Tianjin, 300072, China*

<sup>3</sup>*Institute of Molecular Plus, Tianjin University, Tianjin, 300072, China*

<sup>4</sup>*Department of Electronic and Electrical Engineering, University College London, United Kingdom*

<sup>5</sup>*State Key Laboratory of Millimeter Waves, School of Information Science and Engineering, Southeast University, Nanjing, 210096, China*

<sup>6</sup>*Department of Physics, Imperial College London, London, SW72AZ, United Kingdom*

<sup>7</sup>*Key Laboratory of Micro-Nano Electronic Devices and Smart Systems of Zhejiang Province, College of Information Science and Electronic Engineering, Zhejiang University, Hangzhou, 310027, China*

<sup>8</sup>*feng\_feng@tju.edu.cn*

<sup>9</sup>*xinm@tju.edu.cn*

<sup>10</sup>*weisha@zju.edu.cn*

---

This supplement published with The Optical Society on 4 February 2021 by The Authors under the terms of the [Creative Commons Attribution 4.0 License](https://creativecommons.org/licenses/by/4.0/) in the format provided by the authors and unedited. Further distribution of this work must maintain attribution to the author(s) and the published article's title, journal citation, and DOI.

Supplement DOI: <https://doi.org/10.6084/m9.figshare.13626029>

Parent Article DOI: <https://doi.org/10.1364/OE.414730>

## Supporting Information

### A. CURRENT DISTRIBUTION OF GOLD STRIPS

For the numerical simulations of the current distribution of gold strips, we used the finite-element-method solver under the Electromagnetic Waves, Frequency Domain (ewfd) interface in COMSOL Multiphysics. All calculations are realized for a  $500 \text{ nm} \times 500 \text{ nm}$  unit cell of gold-MoS2 hybrid structure on  $\text{SiO}_2$  substrate (height of  $500 \text{ nm}$ , refractive index  $n = 1.5$ ). The geometry sizes of gold strips were described in the main text in Sec. 2. Material properties for gold was imported from the tabulated data in the reference work<sup>1</sup> mentioned in main text. Corresponding complex permittivity of gold is shown as below:

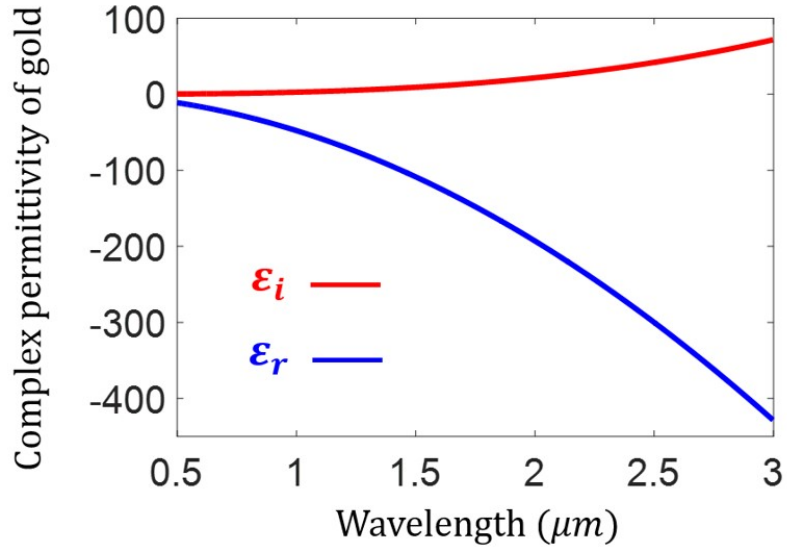


FIG. S1. Real part (blue curve) and imaginary part (red curve) of the dielectric function of gold from the operating wavelength  $500 \text{ nm}$  to  $3000 \text{ nm}$ . The imaginary part is responsible for the loss, and the real part for the degree of polarization of the medium to the external electric field.

Setting with Floquet periodic boundary conditions and one tenth of operating wavelength for the maximum cell size in free space, the optical response of the system was swept from wavelength  $0.5 \mu\text{m}$  to  $3 \mu\text{m}$ . Specifically, the relationship between the electric current density  $\mathbf{J}$ , the magnetic field intensity  $\mathbf{H}$ , and the electric displacement field  $\mathbf{D}$  is given as follows:

$$\nabla \times \mathbf{H} = \frac{\partial \mathbf{D}}{\partial t} + \mathbf{J} \Rightarrow \mathbf{J} = \nabla \times \mathbf{H} - \frac{\partial \mathbf{D}}{\partial t} \Rightarrow \mathbf{J} = \begin{vmatrix} \mathbf{i} & \mathbf{j} & \mathbf{k} \\ \frac{\partial}{\partial x} & \frac{\partial}{\partial y} & \frac{\partial}{\partial z} \\ H_x & H_y & H_z \end{vmatrix} - (-i\omega \mathbf{D}) \quad (\text{S1})$$

Setting the three components of electric current density vector as

$$J_x = \frac{\partial H_z}{\partial y} - \frac{\partial H_y}{\partial z} + i\omega D_x \quad (\text{S2})$$

$$J_y = \frac{\partial H_x}{\partial z} - \frac{\partial H_z}{\partial x} + i\omega D_y \quad (\text{S3})$$

$$J_z = \frac{\partial H_y}{\partial x} - \frac{\partial H_x}{\partial y} + i\omega D_z \quad (\text{S4})$$

Thus the amplitude of the current density can be expressed as  $J = \sqrt{J_x^2 + J_y^2 + J_z^2}$ , and the arrows which indicate the direction of current can be determined via the three components of the current density vector:  $J_x$ ,  $J_y$ , and  $J_z$ .

Sweeping the current distribution from  $0.5 \mu\text{m}$  to  $3 \mu\text{m}$ , we find that the opposite-phase current oscillations occur for the quasi-BIC mode [Fig. 3(a,b)], whereas the in-phase current oscillations occur for the ordinary plasmon-polariton resonance modes [Fig. 2(a,b)]. Current distributions on either side of the quasi-BIC mode  $f_{q-BIC}$  are shown in Fig. S2 below.

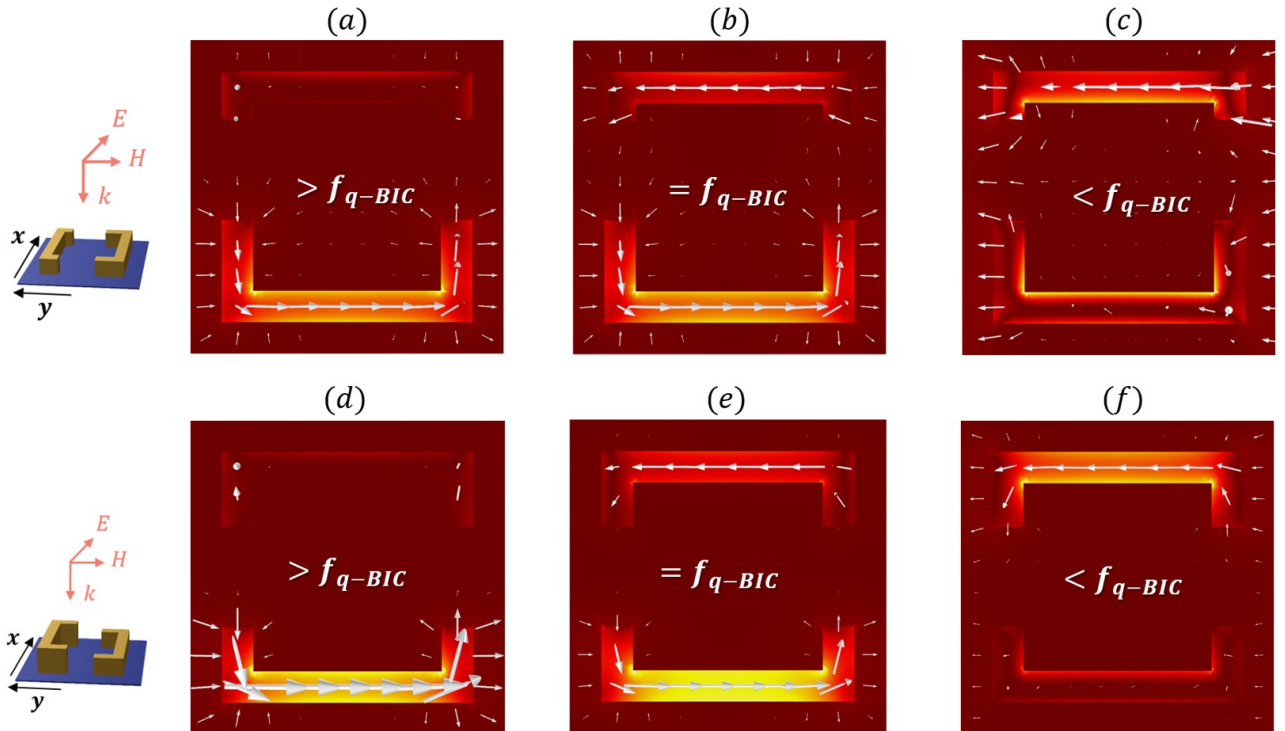


FIG. S2. Evolution of current distribution around the quasi-BIC mode  $f_{q-BIC}$  for (a-c) in-plane and (d-f) out-of-plane symmetry-broken metasurfaces.

For in-plane and out-of-plane asymmetric metasurfaces, there exist transition states for the current distribution [Fig. S2(a,c) and (d,f)] between the quasi-BIC mode (anti-phase current oscillations) and ordinary radiation modes (in-phase current oscillations) of metal structures – the current oscillations disappear on one side of the gold strips around  $f_{q-BIC}$ . This results further confirms the singularity of the quasi-BIC mode of the metasurfaces we proposed in the main text.

## B. BAND STRUCTURE AND Q FACTOR OF BIC-BASED METAMATERIALS

For the numerical calculations of the Q factor and band structure (especially eigenfrequency) of our proposed nanostructure, we employed eigenfrequency solver under the ewfd interface in COMSOL. The model was built in three dimensions, with a unit cell made of gold and MoS<sub>2</sub>. The Floquet periodic conditions are set both in  $x$  and  $y$  directions, and the perfectly matched layers (PML) are constructed in the  $z$  direction.

Due to the dispersive property of the system (the permittivity of gold depends on the frequency), the permittivity is not clear under an unknown eigenfrequency, thus the typical procedure of applying eigenfrequency solver cannot give the right solution. Here the simulation is divided into three steps: (i) For study 1 (ewfd), get the initial solution of eigenfrequency setting with a certain reference value of eigenfrequency; (ii) Set up the constraint condition via ODE function with an integral operator normalizing the E field of the system to ; (iii) For study 2 (ewfd2), utilizing the stationary solver to get the self-consistent solution under the global constraint set in step (ii) (similar approach had also been illustrated in one case from COMSOL application library, but in a simple 2D system – ‘bandgap-photonic-crystal’).

As mentioned in the main text, in order to verify the formation of quasi-BIC mode in the infrared region, we

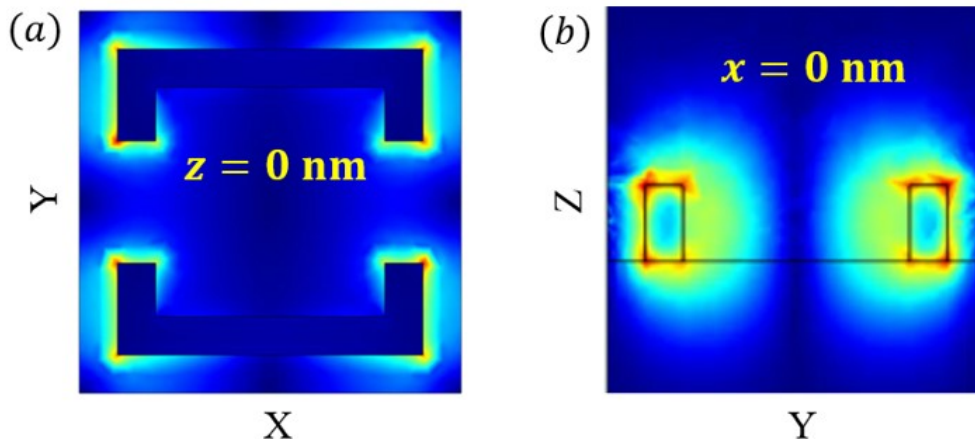


FIG. S3. (a) Calculated eigenfrequencies (including both true and false modes) of our proposed system via COMSOL eigenmode analysis; (b,c) E field distribution at the cut plane when (b)  $z = 0$  nm and (c)  $x = 0$  nm under the BIC-based eigenfrequency ( $f = 1.8466 \times 10^{14}$  Hz in this case).

managed to decrease the imaginary part of permittivity of gold, and thus mitigated the effects of intrinsic metallic losses on the Q factors of the proposed system. Take an instance when imaginary part of permittivity equals to  $10^{-5} \times \epsilon''_{gold}$ , even though there is still little loss in the system, the eigenfrequency at  $\Gamma$  point is real, whereas other ‘false’ eigenmodes calculated by COMSOL all have complex eigenfrequencies [Fig. S3(a)]. This is also another way for judging the true/false eigenmode in COMSOL (the other way is simply to compare the Q factors of these modes).

In addition, to double check our proposed approach of tuning the imaginary part of metallic permittivity is correct, we also plotted the E field profiles [at Fig. S3(b)  $z = 0$  nm and (c)  $x = 0$  nm] under the eigenfrequency  $f = 1.8466 \times 10^{14}$  Hz and  $k = \Gamma$ . We find that the field distributions on  $x$ - $y$  and  $y$ - $z$  plane are the same as the real cases (simulations with actual permittivity of gold). Tuning the imaginary part of gold permittivity would not affect the typical characteristics of metals - localize electromagnetic field on the surface of metals and enhance the localized field by several orders of magnitude.

### C. ACCURACY OF HOMOGENIZATION METHOD

The theoretical method we utilized to extract the effective optical coefficients (especially the effective nonlinear susceptibility) is the improved homogenization technique demonstrated in our previous work<sup>2-5</sup>. Our proposed metasurfaces can be considered as homogenized metasurfaces with effective physical quantities, such as effective permittivities and effective susceptibilities.

To validate the accuracy of the homogenization we applied in the main text, here we compare the optical response (absorbance) of the homogenized metasurfaces with the actual metasurfaces with proposed structures. Based on the constitutive relation of materials, the electric displacement  $\mathbf{D}$  and electric field  $\mathbf{E}$  is expressed as

$$D_i = \sum_j \epsilon_{ij} E_j \quad (S5)$$

where the subscripts  $i, j = x, y, z$ . Thus the averaged fields of the metasurface can be introduced as

$$\mathbf{D}_{eff}(\omega) = \frac{1}{V} \int_V \mathbf{D}(\mathbf{r}, \omega) d\mathbf{r} \quad (S6)$$

$$\mathbf{E}_{eff}(\omega) = \frac{1}{V} \int_V \mathbf{E}(\mathbf{r}, \omega) d\mathbf{r} \quad (S7)$$

where  $V$  is the volume of the unit cell of the metasurface. Thus, utilizing the above equations, the effective electric permittivity of the metasurface can be defined as

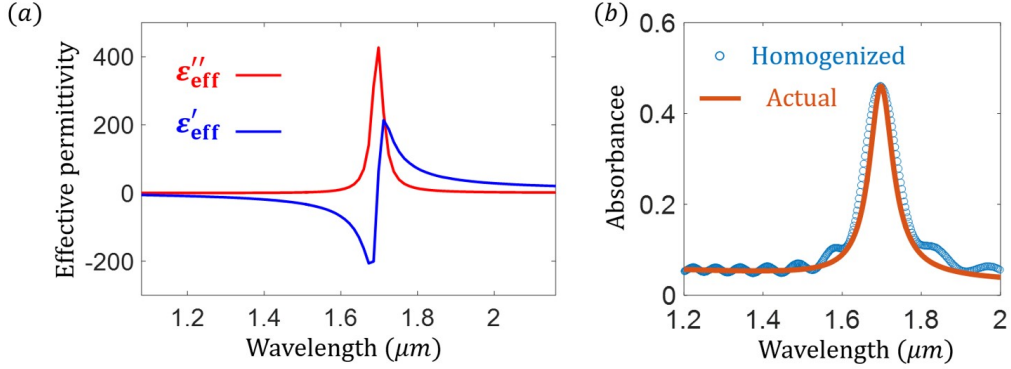


FIG. S4. (a) Effective relative permittivity of the proposed metasurfaces via homogenization approach, with  $L_{y1} = L_{y2} = 120$  nm,  $w = 50$  nm and  $\Delta h = 40$  nm. The real and imaginary part are plotted with blue and red curve, respectively. (b) Absorbance comparison calculated for the actual metasurface (depicted with solid curve) and its homogenized counterpart (marked with circles) with the effective relative permittivity  $\epsilon_{eff}$  plotted in (a).

$$\epsilon_{eff}(\omega) = \frac{\int_V \mathbf{D}(\mathbf{r}, \omega) d\mathbf{r}}{\int_V \mathbf{E}(\mathbf{r}, \omega) d\mathbf{r}} = \frac{\int_V \epsilon(\mathbf{r}) \mathbf{E}(\mathbf{r}, \omega) d\mathbf{r}}{\int_V \mathbf{E}(\mathbf{r}, \omega) d\mathbf{r}} \quad (\text{S8})$$

Calculating the effective permittivity given by Eq. S8, we find that the effective permittivity of the homogenized metasurface presents an evident resonance response at the quasi-BIC mode [Fig. S4(a)], which also verifies the optical enhancing influence brought by metallic plasmons. To assess the validity of the homogenization approach we employed in this work, a reliable way is to compare the optical response (absorbance for instance) between the homogenized structure and the original one. Summarized in Fig. S4(b), the absorbance of the homogenized structure agrees well with the actual metasurface, thus proving the accuracy this homogenization approach in our computations. Note that, for this accuracy test of homogenization, we just used limited number of frequency monitors, leading to weak oscillations in the smooth region of absorbance. When the frequency monitors and meshes in unit cell set in simulations are more enough, the absorbance in these two cases will agree better. Anyway, for the purpose of getting the peak value of effective parameters, the current settings in the simulations are sufficient for us to get the correct results.

#### D. SUGGESTED FABRICATION PROCESS

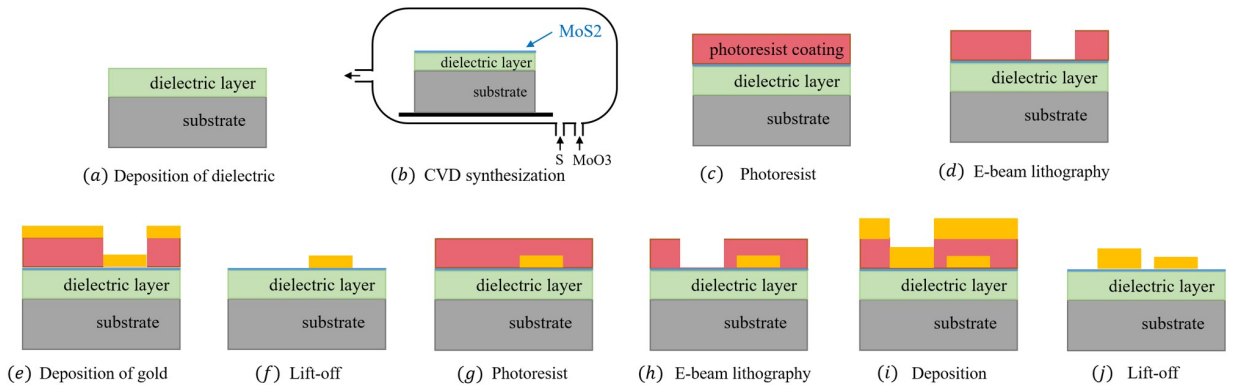


FIG. S5. Suggested fabrication process, including (a-b) the preparation of MoS2 and (c-j) the fabrication of asymmetric metal structures. Structures with different heights can be accomplished by the photoresist coating, EBL, deposition as well as the lift-off processes for twice.

The nanostructure discussed in the paper can be fabricated by the process shown in Fig. 9. The process can be

basically separated into two parts: preparation of MoS<sub>2</sub> monolayers [Fig. 9(a)-(b)] and fabrication of asymmetric metal structures [Fig. 9(c)-(j)]. The MoS<sub>2</sub> monolayer can be synthesized by CVD method. The source of S and Mo comes from sulfur and molybdenum oxide powder, respectively, which could be put into fused quartz tubes of the CVD furnace. The growth of MoS<sub>2</sub> could be carried out under atmospheric pressure and the protection of argon carrier gas. Fabrication of metal structures with different heights (out-of-plane asymmetric structure) can be implemented via the e-beam lithography (EBL) for twice. For instance, in Fig. 9(c)-(j), Au films with different heights are deposited on the MoS<sub>2</sub> monolayer by two independent EBL, with two lift-off processes afterwards. While for in-plane asymmetric structure, only one EBL and one lift-off are needed. Note that another SiO<sub>2</sub> dielectric layer (5 nm) was usually deposited to separate the MoS<sub>2</sub> and metasurface layer for protection, although there was little difference for the final results.

- 
- <sup>1</sup> A. Vial and T. Laroche, "Comparison of gold and silver dispersion laws suitable for FDTD simulations," *Appl. Phys. B* **93**, 139–43 (2008).
  - <sup>2</sup> Q. Ren, J. W. You, and N. C. Panoiu, "Large enhancement of the effective second-order nonlinearity in graphene metasurfaces," *Phys. Rev. B* **99**, 205404 (2019).
  - <sup>3</sup> Q. Ren, J. W. You and N. C. Panoiu, "Giant enhancement of the effective Raman susceptibility in metasurfaces made of silicon photonic crystal nanocavities," *Opt. Express* **26**, 30383-30392 (2018).
  - <sup>4</sup> J. W. You, E. Threlfall, D. F. Gallagher, and N. C. Panoiu, "Computational analysis of dispersive and nonlinear 2D materials by using a GS-FDTD method," *J. Opt. Soc. Am. B* **35**, 2754-2763 (2018).
  - <sup>5</sup> J. W. You and N. C. Panoiu, "Plasmon-induced nonlinearity enhancement and homogenization of graphene metasurfaces," *Opt. Lett.* **44**, 3030-3033 (2019).